Noname manuscript No.
(will be inserted by the editor)

Combinatorial Optimization of the Discretized Multiphase Mumford-Shah Functional

Noha Youssry El-Zehiry · Leo Grady

Received: date / Accepted: date

Abstract The Mumford-Shah model has been one of the most influential models in image segmentation and denoising. The optimization of the multiphase Mumford-Shah energy functional has been performed using level sets methods that optimize the Mumford-Shah energy by evolving the level sets via the gradient descent. These methods are very slow and prone to getting stuck in local optima due to the use of gradient descent. After the reformulation of the 2-phase Mumford-Shah functional on a graph, several groups investigated the hierarchical extension of the graph representation to multi class. The discrete hierarchical approaches are more effective than hierarchical (or direct) multiphase formulation using level sets. However, they provide approximate solutions and can diverge away from the optimal solution. In this paper, we present a discrete alternating optimization for the discretized Vese-Chan approximation of the piecewise constant multiphase Mumford-Shah functional that directly minimizes the multiphase functional without recursive bisection on the labels. Our approach handles the nonsubmodularity of the multiphase energy function and provides a global optimum if the image estimation data term is known apriori.

Keywords Multiphase Mumford-Shah · Discrete Optimization · Image Segmentation · Image Denoising

Noha Youssry El-Zehiry
Siemens Corporation, Corporate Technology
Imaging and Computer Vision
Princeton, NJ, USA.
E-mail: noha.el-zehiry@siemens.com

Leo Grady
HeartFlow Inc.
Redwood city, CA, USA.
E-mail: leograd@yahoo.com

1 Introduction

The formulation of the image segmentation problem as an energy minimization problem has been one of the most powerful and commonly used techniques in the past couple of decades. For example, the piecewise constant Mumford-Shah segmentation aims at minimizing the integral of the intensity deviations around the mean of each class.

Minimizing such integral equations can be done in two ways (Bruckstein et al, 1997): First, to find the associated partial differential equation and use numerical methods to solve the PDE, in which case, discretization of the solution domain is used to optimize the continuous problem. An alternative method is to find the analogous discrete problem and employ combinatorial optimization tools to solve it. Numerical solution of PDE's via level sets method has been extensively used in image segmentation. However, it suffers from several drawbacks such as: 1) it requires tuning for many parameters. When different parameters are used to discretize the solution domain, the results may vastly change. 2) It depends on local optimization tools such as the gradient descent method for the optimization of the continuous problem, but these are known to get stuck in local optima and jeopardize the quality of the output.

Recent studies (El-Zehiry et al, 2011; Grady and Alvino, 2009; Darbon and Sigelle, 2005) demonstrate the favorability of the discrete approach. They unify two of the most important frameworks in image segmentation: graph representation and variational formulations. The ultimate goal of the new hybrid framework is to provide new discrete formulations that can benefit from the arsenal of variational formulations literature and meanwhile extend the robustness of these algorithms by employing combinatorial optimization al-

gorithms that can capture global optima in a relatively very short time.

In this paper, we extend the work of El-Zehiry et al (2011) and Grady and Alvino (2009) by investigating the combinatorial optimization of the multiphase Mumford - Shah energy functional and demonstrate its application to image segmentation and brain MRI tissue classification. We will present a discrete formulation of the multiphase piecewise constant Mumford-Shah segmentation functional and provide a graph construction that represents the discrete energy function. We then discuss the nonsubmodularity of the resulting function and employ Quadratic Pseudo Boolean Optimization (QPBO) introduced by Hammer et al (1984), Kolmogorov and Rother (2007) and Quadratic Pseudo Boolean Optimization with Probing (QPBOP) of Rother et al (2007) to minimize the resulting discrete energy function. The minimization scheme is an iterative alternating scheme that alternates between two main components: the first is calculating the data priors of the discretized Mumford-Shah energy functional, the second is optimization of the boundary between the segments, represented by labeling. In our formulation, each iteration solves globally the boundary optimization for a multilabel graph cut problem (up to four labels). We will present the results of our algorithm on scalar and vector valued image segmentation for synthetic and real images. The paper also investigates the feasibility of extending our formulation to more than four labels. We will discuss the challenges associated with this extension.

1.1 The Multiphase Mumford-Shah Model

The multiphase Mumford-Shah model is generalization of the 2-phase. This generalization plays an important role in different applications such as segmenting images that contain more than a single object, coloring maps with different regions or clustering data to more than two clusters.

The multiphase Mumford-Shah functional for image segmentation problem can be summarized as follows: Let Ω be an open bounded set in $\mathbb{R}^2$. Let C be a closed subset of Ω consisting of a finite set of smooth curves. The set $\Omega \backslash C$ is composed of a partition of disjoint connected components denoted as ω_i such that $\Omega = \cup_i \omega_i \cup C$. The segmentation problem can be described as finding a piecewise smooth approximation u_d of an input image u such that u_d varies smoothly inside each connected components ω_i with sharp transitions between the different components.

Mumford and Shah (1988) proposed that the optimal segmentation can be obtained by minimizing the following energy

$$F_{MS}(u_d, C) = \int_{\Omega} (u - u_d)^2 \, dxdy + \mu \int_{\Omega \backslash C} |\nabla u_d| \, dxdy + \nu |C|, \quad (1)$$

where μ and ν are weighting parameters used to control the contribution of each term in the energy function. The piecewise constant Mumford-Shah model is a simpler model obtained by assuming that image approximation is constant inside each connected component (*i.e.* $u_d = c_i$ where c_i is a constant). This results in the following simplified energy functional:

$$F_{MS}(c_i, C) = \sum_{i=1}^{m} \int_{\omega_i} (u - c_i)^2 + \nu |C|, \quad (2)$$

where m is the number of connected components. Notice that the 2-phase Mumford-Shah model is a special case of (2) where $m = 2$. The next subsection will review the previous work on optimizing the multiphase Mumford-Shah model.

1.2 Previous work

In this section, we review the previous work on the optimization of the multiphase Mumford-Shah functional in the continuous and discrete optimization literature. We will also discuss the relationship between the Mumford-Shah segmentation model for multiple classes and the multilabel partitioning problem as well as the optimization of the q-potts model for $q > 2$.
The optimization of the multiphase Mumford - Shah model has been previously investigated by several research groups, either in a continuous framework (Vese and Chan, 2002; Ni et al, 2009; Jeon et al, 2005) or discrete framework (El-Zehiry and Elmaghraby, 2007; Bae and Tai, 2009a,b). Most of the continuous approaches are slow and do not provide a global optimal solution. Even the most recent recursive approach of Ni et al (2009) that used an efficient global optimization for the 2-phase Mumford-Shah presented by Bresson et al (2007) does not guarantee the global optimality of the multiphase function due to the recursive nature of the solution.

Despite the recent advancement of combinatorial optimization schemes that yield global optima and exhibit low computational complexity, several problem

formulations are still suffering from local solutions associated with gradient descent solutions or recursive bisection schemes. In addition to local optimality, the implementation of such schemes often comes at a very high computational cost that limits the applicability of such algorithms. Recent examples of such models include Ni et al (2009), Badshah and Chen (2009) and Vazquez-Reina et al (2009). This striking fact urged us to investigate the fast and global optimization of the Mumford-Shah multiphase energy function that can be achieved by optimizing the corresponding discrete functional on a graph using QPBO/QPBOP.

The extension of the discrete optimization of the 2-phase Mumford - Shah model to multiphase is not straightforward. This is due to the nonsubmodularity of the resulting discrete energy function. This problem has been investigated by El-Zehiry and Elmaghraby (2007) and Bae and Tai (2009b). The previous contributions presented a graph cut optimization of the multiphase Mumford-Shah functional through a sequence of binary segmentation steps. These recursive approaches are approximate and, in certain scenarios, they may produce solutions that are very far from the optimal solution as shown by Simon and Teng (2001). Unlike Bae and Tai (2009b) and El-Zehiry and Elmaghraby (2007), in this paper we globally solve the 4-label boundary optimization by directly minimizing the multiphase energy function itself.

From a broader perspective, the multiphase Mumford - Shah image segmentation can be seen as a special case of the multilabel partitioning problem. The latter refers to subdividing the image into several partitions, where each partition represents an object or an area of interest. This problem can be solved in a continuous setting or discrete setting. In the continuous setting, variational formulations of the multilabel partitioning problem aim at subdividing an open set Ω that corresponds to the image domain into disjoint subregions $\{\omega_i\}_{i=1}^{n}$ that correspond to the multiple partitions by minimizing a predefined energy function. The energy function consists of a data fidelity term inside each ω_i and a regularization term on the boundaries. The level set method developed by Osher and Sethian (1988) has been one of the most dominant tools used for the numerical implementation and optimization of such variational formulations e.g. (Vese and Chan, 2002; Chung and Vese, 2005). Such methods generally use gradient descent in the optimization step leading to approximate local solutions. Other continuous approaches tend to do the approximation in the model rather than the optimization scheme. For example, some algorithms convexify the problem to get a new convex energy that can be optimized globally and exactly (Pock et al, 2008, 2009; Lellmann et al, 2009; Yuan et al, 2011; Brown et al, 2010). However, the global exact solution to the convex problem is just an approximate solution to the original nonconvex problem (Pock et al, 2008).

In a discrete setting, each pixel in the image is associated with a vertex in a graph. The multilabel partitioning energy is used to assign the weights on the graph. The terminal weights (between the graph vertices and terminal vertices) are usually assigned based on the data energy and the edge weights either pairwise (Boykov et al, 1999) or with higher order cliques (Kohli et al, 2009), reflect the boundary smoothness or the regularities in assigning weights. The general graph partitioning problem for more than two labels correspond to solving a q-Potts model with $q > 2$ or solving a multiway cut problem which are generally NP-hard. Hence, several algorithms try to either solve the problem in special cases that are not NP-hard e.g. (Ishikawa, 2003). Other approaches solve the problem by approximation. The approximation can be done by either finding a suboptimal solution to the q-Potts model problem such as the $\alpha - \beta$ swap solution presented by Boykov et al (1999), or relaxation methods of Komodakis and Tziritas (2007); Wainwright et al (2002). Other solutions approximate the NP-hard problem and finds a global solution for the approximated problem as presented by Bae and Tai (2009a). Bae et al (2011) also presented a global minimization of the multiphase segmentation problem by convexifying the continuous variant of the Potts model. They have investigated the convex relaxation of the continuous Potts model and presented the equivalence with the primal-dual formulations of the relaxation. They introduced smoothing to the dual formulation and showed that the solution to the relaxed problem often yields the global solution to the original nonconvex problem. The next few paragraphs highlight in more depth the differences between our paper and the most relevant approaches of Delong and Boykov (2009); Ramalingam et al (2008); Bae and Tai (2009a).

Recently, Delong and Boykov (2009) presented an approach for multi-region image segmentation. They build a graph of n layers to segment n classes and assign inter-layer links with weights which depend on the geometric interactions among the distinct classes. The authors dissected the geometric interactions between two classes into 3 main categories: 1) Containment- Where one region A contains all the pixels of region B. 2) Exclusion- Where the two regions A and B cannot overlap in any of the pixels. 3) Attraction- Where the area A-B exterior to B is penalized by a given positive cost. The authors explained how the combinations between these interactions can usually be converted to submodular or supermodular interactions that can be optimized

globally using graph cuts. However, in more difficult cases, the combination results in nonsubmodulatirty in which case the authors either truncate the nonsubmodular terms or provide approximate solutions. Similar to Delong and Boykov (2009), we construct a multi-layer graph, however, we use only $\log_2 n$ layers to segment n classes. Our construction does not allow to model geometric constraints between labels of different pixels. However, it implicitly places constraints on the labels of the layer variables corresponding to the same pixel. In particular, a problem where segment A must include disjoint segments B and C is implicitly modeled by identifying B with layer variables combination 10, C with 11 and A with 1*. The inter-layer interactions in our model originate from the data and need not be submodular. This special case of the model by Delong and Boykov was indicated as difficult, however, in our reformulation we successfully solve it with QPBOP, see row 3 of Figure 4. Notice that the regions A, B and C in this figure correspond to the sky, trees and moon, respectively. The sky contains the trees and the moon but the moon excludes the trees.

Binary encoding of multi-label problems has been discussed by Ramalingam et al (2008); Bae and Tai (2009b). In the approach of Ramalingam et al (2008), 2 or more Boolean variables are used to to encode the states of a single multi-label variable. For example, to encode a problem of a four class labeling, they used the battleship transformation of Ishikawa (2003) that utilizes three Boolean variables. The resulting binary interaction of the battleship transformation is submodular. In our paper, we will use only two variables, similar to Bae and Tai (2009a); El-Zehiry (2009), instead of three to encode a four class labeling problem. The price of using less variables is that the resulting function will be nonsubmodular.

While our work also discusses the problem of multilabel partitioning, unlike Delong and Boykov (2009) and Ramalingam et al (2008), we present a reformulation of the multiphase Mumford-Shah problem that is commonly used in different imaging applications. Our work will improve the speed and quality of any application that uses the multiphase Mumford-Shah Model or Vese-Chan Model.

Bae and Tai (2009a) used fewer Boolean variables than Ramalingam et al (2008). We independently developed a graph construction similar to the construction proposed in Bae and Tai (2009a) where the graph is constructed in layers and every layer correspond to a binary variable such that the final class labeling is obtained by combining these labels for the different variables. However, they proposed a constraint on the relationship between the mean intensity values of the distinct classes to guarantee the submodularity of the multiphase functional (which is not guaranteed to be satisfied in all input images). For example, in the case of 4-class segmentation investigated in Bae and Tai (2009a), it is necessary to choose the appearance priors $f_1 = (u - c_1)^2$, $f_2 = (u - c_2)^2$, $f_3 = (u - c_3)^2$ and $f_4 = (u - c_4)^2$ such that $c_1 < c_2 < c_3 < c_4$ and satisfying the following inequality to guarantee the submodularity of the energy.

$$|c_2 - u|^2 + |c_3 - u|^2 \leq |c_1 - u|^2 + |c_4 - u|^2. \quad (3)$$

If this constraint is not satisfied, they handle the optimization by multi-step case analysis of the constructed graph. However, in our approach, we do not restrict the input domain but instead we deal with the nonsubmodularity of the multiphase function using QPBO and QPBOP (Rother et al, 2007; Boros et al, 2006). The authors claim that if the class means are not evenly distributed, the submodularity is violated if large regularization values are used but we would like to highlight that if only low regularization values are used then the problem is reduced to a simple thresholding problem. High regularization values may be necessary for practical applications. The results section will show that our works equally well for low and high regularization values. Moreover, Bae and Tai did not discuss the 3-phase segmentation in their work, which we will address later in our paper.

Graph cuts, the most commonly used combinatorial optimization tool in vision, provides complete global solutions only if the function to be optimized is submodular. Hence, contributions towards solving the multiphase segmentation problem, e.g. (Bae and Tai, 2009a; El-Zehiry and Elmaghraby, 2007) aim at avoiding nonsubmodularity, sometimes at very high cost. However, we believe that with the recent advancement in combinatorial optimization and the introduction of QPBO /QPBOP, researchers are urged to overlook the submodularity constraint and start dealing directly with nonsubmodular functions and use these powerful tools for the optimization. Although QBPO and QBPOP are not guaranteed, theoretically, to provide complete solution, we found them very effective in practice as we will discuss in the results section.

The rest of the paper is organized as follows: Section 2 will review the Vese and Chan (2002) level set formulation for the multiphase piecewise constant Mumford-Shah functional. We will present the discrete formulation of the energy function and provide the graph construction and the optimization details of the discrete energy function. We also introduce two extensions: The first extension relaxes the homogeneity constraint and introduces a smoother modeling of the images. The second extension explains how to generalize the formu-

lation to vector valued images in the discrete setting. The section will also present the graph construction, proposed optimization and discuss the challenges associated with generalizing the model to more than 4 classes. Section 3 will introduce a sample of our segmentation results to synthetic and real images, it will also depict results for MRI tissue classification. Finally, Section 4 will conclude the paper and present insights for future improvements.

2 Methods

We start this section by reviewing the Vese-Chan level set formulation for the multiphase image segmentation problem and we proceed to the discrete formulation of the piecewise constant model, its extension to a locally constant model and handling of vector-valued images. Finally, the optimization using Quadratic Pseudo Boolean Optimization and Quadratic Pseudo Boolean Optimization with Probing and details of the algorithm will be presented. We will also discuss the generalization of the model to more than 4 classes.

2.1 Review of Level Set Formulation of the Multiphase Piecewise Constant Mumford-Shah model

This section will review the multiphase image segmentation approach presented by Vese and Chan (2002). Vese and Chan proved, using the four color theorem, that four classes are sufficient to provide labeling for any number of objects in 2D. This also applies to partitioning any planar graph. Following their reasoning, we will only focus on four and three class segmentation. Vese and Chan have presented a multiphase image segmentation approach using level sets of Vese and Chan (2002). Their multiphase image segmentation approach extends their model of Chan and Vese (2001) by using several level set functions instead of one. One level set function can only separate two classes, hence $n_1 = \log_2 n$ is the number of level sets necessary to segment n distinct classes. Figures 1 illustrates how two level set functions separate four classes.

Two level set functions ϕ_1 and ϕ_2 are used to span the input domain Ω such that $\Omega = \bigcup_{i=1}^{4} \omega_i$ where:

$$\begin{aligned}
\omega_1 &= \{p \mid \phi_1(p) > 0 \text{ and } \phi_2(p) > 0\},\\
\omega_2 &= \{p \mid \phi_1(p) > 0 \text{ and } \phi_2(p) < 0\},\\
\omega_3 &= \{p \mid \phi_1(p) < 0 \text{ and } \phi_2(p) > 0\},\\
\omega_4 &= \{p \mid \phi_1(p) < 0 \text{ and } \phi_2(p) < 0\}.
\end{aligned}$$

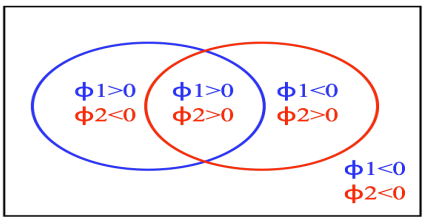

Fig. 1 Two evolving contours represented by two level set functions $\phi_1 = 0$ and $\phi_2 = 0$.
The two level set functions subdivide the domain into 4 regions;$\{\phi_1 > 0, \phi_2 > 0\}, \{\phi_1 > 0, \phi_2 < 0\}, \{\phi_1 < 0, \phi_2 > 0\}$ and $\{\phi_1 < 0, \phi_2 < 0\}$. Courtesy of Vese and Chan (2002)

And the set of closed curves C is defined as

$$C = \{p | \phi_1(p) = 0 \text{ or } \phi_2(p) = 0\}. \tag{4}$$

In Vese and Chan (2002), the authors perform the segmentation task by minimizing the intensity deviation around the class means and minimizing the length of every level set as a regularization.

The mean intensities inside each of the previous regions are represented by the vector $C = [c_{11}\ c_{10}\ c_{01}\ c_{00}]$. Hence the segmentation can be obtained by minimizing the energy functional in Vese and Chan (2002) represented by the following formulation;

$$\begin{aligned}
F(\phi_1, \phi_2) = &\int_\Omega (u - c_{11})^2 H(\phi_1) H(\phi_2) dxdy\\
&+ \int_\Omega (u - c_{01})^2 (1 - H(\phi_1)) H(\phi_2) dxdy\\
&+ \int_\Omega (u - c_{10})^2 H(\phi_1)(1 - H(\phi_2)) dxdy\\
&+ \int_\Omega (u - c_{00})^2 H(1 - \phi_1)(1 - H(\phi_2)) dxdy\\
&+ \nu_1 \int_\Omega |\nabla H(\phi_1)| dxdy + \nu_2 \int_\Omega |\nabla H(\phi_2)| dxdy.
\end{aligned} \tag{5}$$

The parameters ν_1 and ν_2 are weighting factors that control the length contribution in every level set and $H(\phi)$ is the Heaviside step function of the level set ϕ.

2.2 Discrete Formulation

To provide a discrete formulation for the multiphase segmentation energy in (5), each pixel $p \in \Omega$ will be associated with a vector of binary variables $X_p = [x_p\ y_p]$. The vector components are defined as follows:

$$x_p = \begin{cases} 1, \phi_1(p) > 0; \\ 0, \text{otherwise.} \end{cases} \tag{6}$$

$$y_p = \begin{cases} 1, \phi_2(p) > 0; \\ 0, \text{otherwise.} \end{cases} \quad (7)$$

Hence, $X_p \in \{[1\ 1],\ [0\ 1],\ [1\ 0],\ [0\ 0]\}$ and the labeling for the different classes ω_1, ω_2, ω_3 and ω_4 are 11, 01, 10 and 00, respectively.

To discretize (5), each integral may be viewed as a chain paired with a cochain. The image intensities are viewed as a 0-cochain and every pixel will be associated with a vertex in the graph. More details about the discrete representation of differential operators have been presented by Grady and Polimeni (2010).

The discrete formulation of the segmentation energy is given by the discrete function F_D expressed as:

$$F_{\mathrm{D}} = F_{\mathrm{Data}} + \nu_1\, F_{\mathrm{L}_1} + \nu_2\, F_{\mathrm{L}_2}. \quad (8)$$

Generally, the data and its fidelity can vastly vary depending on the problem of interest. By introducing our formulation on an arbitrary graph it is possible to apply the multiphase MS to problems beyond image segmentation, such as data clustering.

In this paper, we will discuss three different data models: The piecewise constant data model presented in Section 2.1 for scalar images (F_{DataPC}), a locally constant data model for scalar images (F_{DataPS}) and the extension of the previous models to vector-valued images (F_{DataVV}) will be presented in Sections 2.3 and 2.4, respectively.

We start with the piecewise constant Mumford-Shah data fidelity with a target application of multiphase 2D scalar image segmentation, in which case, $F_{\mathrm{Data}} = F_{\mathrm{DataPC}}$, F_{L_1} and F_{L_2} are defined as follows:

$$\begin{aligned} F_{\mathrm{DataPC}} = & \sum_{p\in\Omega} (u(p) - c_{11})^2 x_p y_p \\ & + \sum_{p\in\Omega} (u(p) - c_{01})^2 (1 - x_p) y_p \\ & + \sum_{p\in\Omega} (u(p) - c_{10})^2 x_p (1 - y_p) \\ & + \sum_{p\in\Omega} (u(p) - c_{00})^2 (1 - x_p)(1 - y_p), \end{aligned} \quad (9)$$

$$F_{L_1} = \sum_{p\in\Omega} \sum_{q\in\mathcal{N}(p)} |x_p - x_q| w_{pq}, \quad (10)$$

$$F_{L_2} = \sum_{p\in\Omega} \sum_{q\in\mathcal{N}(p)} |y_p - y_q| w_{pq}, \quad (11)$$

where $p = (x, y)$ represents an image pixel and the c_{00}, c_{01}, c_{10} and c_{11} are the mean intensity values of the classes ω_1, ω_2, ω_3 and ω_4, respectively. Notice that the set Ω now refers to a discrete set of pixels. The set $\mathcal{N}(p)$ represents the set of nodes in the neighborhood of p and w_{pq} is the weight of the edge $v_p v_q$ that represents a discrete representation of the Euclidean boundary length, details have been presented in the previous work of Kolmogorov and Boykov (2005); El-Zehiry et al (2007). Notice that this formulation double counts the length penalty at the boundaries between ω_1 and ω_4 and the boundaries between ω_2 and ω_3. However, this is an inherent problem from the continuous formulation that carries over to our discrete formulation. Notice that this approximation of the length makes the formulation different from the Potts model for graph partitioning as in Potts model, discontinuities between any pair of labels are penalized equally. Since the problem deviates from the q-Potts (with $q > 2$) model, our formulation is not NP-hard. This enables us to obtain a global solution for 3 and 4 class segmentation.

The mean intensities are expressed as follows:

$$c_{11} = \frac{\sum_{p\in\Omega} u(p)\ x_p y_p}{\sum_{p\in\Omega}\ x_p y_p} \quad (12)$$

$$c_{01} = \frac{\sum_{p\in\Omega} u(p)\ (1 - x_p) y_p}{\sum_{p\in\Omega} (1 - x_p) y_p} \quad (13)$$

$$c_{10} = \frac{\sum_{p\in\Omega} u(p)\ x_p (1 - y_p)}{\sum_{p\in\Omega}\ x_p (1 - y_p)} \quad (14)$$

$$c_{00} = \frac{\sum_{p\in\Omega} u(p)\ (1 - x_p)(1 - y_p)}{\sum_{p\in\Omega} (1 - x_p)(1 - y_p)} \quad (15)$$

The image can be approximated by the piecewise constant model

$$\begin{aligned} u_d(p) = & \ c_{11}\, x_p y_p + \ c_{01}\, (1 - x_p) y_p \\ & + \ c_{10}\, x_p (1 - y_p) + \ c_{00} (1 - x_p)(1 - y_p) \end{aligned} \quad (16)$$

The piecewise constant approximation works well for homogeneous images where the variation of intensities inside every class is limited. The next subsection explains how to relax the homogeneity constraint to handle images with higher intensity variations.

2.3 Extension to a Locally Constant Mumford-Shah Model

The previous formulation approximates the four classes of the image by four global means c_{00}, c_{01}, c_{10} and c_{11}. This approximation is valid under the assumption that the image is homogeneous and the intensity model is piecewise constant. In practice, this assumption is sometimes violated. To relax the homogeneity constraint, we associate every pixel p in the image with four local means $m_{00}(p)$, $m_{01}(p)$, $m_{10}(p)$ and $m_{11}(p)$ to represent

the mean intensity values in the vicinity of the pixel p and inside the respective classes ω_1, ω_2, ω_3 and ω_4. This is a simple approximation to a smoother modeling of the image. It has been proven efficient in practice by El-Zehiry and Elmaghraby (2008). The local means are defined as:

$$m_{11}(p) = \frac{\sum_{\mathcal{W}} u(p)x_p y_p}{\sum_{\mathcal{W}} x_p y_p}, \tag{17}$$

$$m_{01}(p) = \frac{\sum_{\mathcal{W}} u(p)(1-x_p) y_p}{\sum_{\mathcal{W}} (1-x_p) y_p}, \tag{18}$$

$$m_{10}(p) = \frac{\sum_{\mathcal{W}} u(p)x_p (1-y_p)}{\sum_{\mathcal{W}} x_p (1-y_p)}, \tag{19}$$

$$m_{00}(p) = \frac{\sum_{\mathcal{W}} u(p)(1-x_p)(1-y_p)}{\sum_{\mathcal{W}} (1-x_p)(1-y_p)}. \tag{20}$$

where $\mathcal{W}$ is a predefined neighborhood of the pixel p. In the experiments, we will use a rectangular window of size $2k+1$ centered at the pixel p and k is a constant. The data term is then modified to be as follows:

$$\begin{aligned} F_{\text{DataPS}} &= \sum_{p\in\Omega} (u(p) - m_{11}(p))^2 x_p y_p \\ &+ \sum_{p\in\Omega} (u(p) - m_{01}(p))^2 (1-x_p) y_p \\ &+ \sum_{p\in\Omega} (u(p) - m_{10}(p))^2 x_p (1-y_{p)} \\ &+ \sum_{p\in\Omega} (u(p) - m_{00}(p))^2 (1-x_p)(1-y_p). \end{aligned} \tag{21}$$

and the smooth approximation of the model is expressed as

$$\begin{aligned} u_d(p) = m_{11}(p)\ \ x_p y_p + m_{01}(p)\ \ (1-x_p) y_p \\ + m_{10}(p)\ \ x_p (1-y_p) + m_{00}(p)\ \ (1-x_p)(1-y_p). \end{aligned} \tag{22}$$

Notice that if the window size is infinite, then $\mathcal{W} = \Omega$ and $m_{11}(p) = c_{11}$, $m_{10}(p) = c_{10}$, $m_{01}(p) = c_{01}$ and $m_{00}(p) = c_{00}$ $\forall p \in \Omega$. In other words, if the window size is large enough, local means become global and the piecewise constant approximation may be viewed as a special case of the locally constant approximation.

2.4 Extension to Segmentation of Vector Valued Images

This section introduces a natural extension of the proposed segmentation model in Section 2.2 to handle vector valued images. Let $u(p,i)$ be the intensity value of the spatial coordinates $p = (x,y)$ in the i channel with $i \in \{1,2,...,N\}$ where N is the number of channels in the input image.

The different channels contain the same image with different information, for example, the RGB components of a color image or different wavelength at which the image is captured. $\overline{c_{11}} = (c_{1\_11}, c_{2\_11}, ..., c_{N\_11})$ is a vector of the mean intensity value inside ω_1 for the different channels. Similarly, $\overline{c_{01}} = (c_{1\_01}, ..., c_{N\_01})$, $\overline{c_{10}} = (c_{1\_10}, ..., c_{N\_10})$ and $\overline{c_{00}} = (c_{1\_00}, ..., c_{N\_00})$ are the vectors of mean intensity values in ω_2, ω_3 and ω_4, respectively. The extension to the vector valued case can be represented by minimizing the energy function $F = F_{DataVV} + F_{L1} + F_{L2}$ where

$$\begin{aligned} F_{\text{DataVV}} &= \sum_{p\in\Omega} \left(\frac{1}{N} \sum_{i=1}^{N} |u(p,i) - c_{i\_11}|^2 \right) x_p y_p \\ &+ \sum_{p\in\Omega} \left(\frac{1}{N} \sum_{i=1}^{N} |u(p,i) - c_{i\_01}|^2 \right) (1-x_p) y_p \\ &+ \sum_{p\in\Omega} \left(\frac{1}{N} \sum_{i=1}^{N} |u(p,i) - c_{i\_10}|^2 \right) x_p (1-y_p) \\ &+ \sum_{p\in\Omega} \left(\frac{1}{N} \sum_{i=1}^{N} |u(p,i) - c_{i\_00}|^2 \right) (1-x_p)(1-y_p). \end{aligned} \tag{23}$$

The regularization is still represented by F_{L1} and F_{L2} defined in (10) and (11). The values of c_{i_11}, c_{i_01}, c_{i_10} and c_{i_11} are updated according to the new labels using the following formulas:

$$c_{i\_11} = \frac{\sum_{p\in\Omega} u(p,i) x_p y_p}{\sum_{p\in\Omega} x_p y_p}, \tag{24}$$

$$c_{i\_01} = \frac{\sum_{p\in\Omega} u(p,i)(1-x_p) y_p}{\sum_{p\in\Omega} (1-x_p) y_p}, \tag{25}$$

$$c_{i\_10} = \frac{\sum_{p\in\Omega} u(p,i) x_p (1-y_p)}{\sum_{p\in\Omega} x_p (1-y_p)}, \tag{26}$$

$$c_{i\_00} = \frac{\sum_{p\in\Omega} u(p,i)(1-x_p)(1-y_p)}{\sum_{p\in\Omega} (1-x_p)(1-y_p)}. \tag{27}$$

After minimizing the energy, the piecewise constant model approximation is estimated by calculating the norm of the mean intensity values inside the different classes resulting in the following image model:

$$\begin{aligned} u_d(p) = \sqrt{\frac{\sum_{i=1}^{N} c_{i\_11}^2}{N}}\ \ x_p y_p + \sqrt{\frac{\sum_{i=1}^{N} c_{i\_01}^2}{N}}\ \ (1-x_p) y_p \\ + \sqrt{\frac{\sum_{i=1}^{N} c_{i\_10}^2}{N}}\ \ x_p (1-y_p) + \sqrt{\frac{\sum_{i=1}^{N} c_{i\_00}^2}{N}}\ \ (1-x_p)(1-y_p) \end{aligned} \tag{28}$$

Notice that the locally constant image model in Section 2.3 can also be integrated to the vector-valued data term by using local means in each channel.

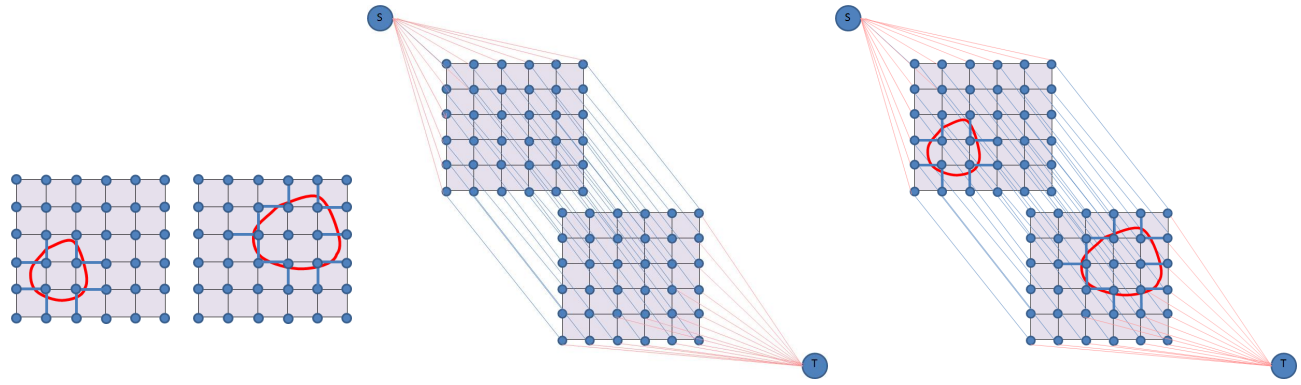

(a) $\mathcal{G}_1$ (b) $\mathcal{G}_2$ (c) $\mathcal{G}_3$ (d) $\mathcal{G}$

Fig. 2 Graph construction. (a) $\mathcal{G}_1$, the graph that represents F_{L1}, (b) $\mathcal{G}_2$, the graph that represents F_{L2}, (c) $\mathcal{G}_3$, the graph that represents F_{Data} and (d) The final graph that represents F_D.

To optimize the function in (8), every binary variable will be associated with a vertex in the graph. The vertices will be arranged in two layers, one layer with the vertices corresponding to x_p and another for the vertices representing y_p as shown in Figure 2. The intra-layer links will be determined based on the F_{L1} and F_{L2} and the inter-layer links will be determined according to F_{Data} (more details in the next section). El-Zehiry and Elmaghraby (2007) and Bae and Tai (2009b) have investigated the graph cut optimization of the multiphase Vese-Chan model. However, the discrete model in (9) violates the submodularity constraint presented by Kolmogorov and Zabih (2004) which made the graph optimization of the energy function very challenging. In the previous contributions, the authors presented a hierarchical approach to solve the multiphase segmentation problem by applying a sequence of binary segmentation steps. Bae and Tai (2009a) investigated the direct unhierarchical optimization of the discrete model in (9) but their approach works well if the data priors are chosen such that the constraint in (3) is satisfied, in which case the energy function is guaranteed to be submodular and graph cuts can be directly used to minimize it. In our paper, we use a similar graph construction but we do not restrict the data priors and we do not require the energy function to be submodular. With the advances in the discrete optimization field and the contributions of Kolmogorov and Rother (2007); Rother et al (2007), we propose to solve the multiphase segmentation problem in a non sequential manner that reduces the time complexity of the segmentation and improves the robustness of the model. We minimize the non submodular function using QPBO and QPBOP. The next subsection will present the discrete optimization of the proposed energy function using Quadratic Pseudo Boolean Optimization.

2.5 Discrete Optimization

Kolmogorov and Rother (2007) have reviewed the minimization of nonsubmodular functions using Quadratic Pseudo Boolean Optimization, an approach that was first introduced in the optimization literature by in Hammer et al (1984). Similar to graph cuts methods, QPBO works by reducing the problem to the computation of a min $\mathcal{S}$-$\mathcal{T}$ cut but with two fundamental differences. First, the constructed graph contains double the number of vertices, since for every variable x two vertices are added to the graph producing the vertex set $\mathcal{V} = \{v_x, v_{\overline{x}} | x \in X\}$ and, in general, QPBO provides partial labeling for the vertices such that

$$x = \begin{cases} 0, & v_x \in \mathcal{S},\ v_{\overline{x}} \in \mathcal{T}, \\ 1, & v_x \in \mathcal{T},\ v_{\overline{x}} \in \mathcal{S}, \\ \emptyset, & \text{otherwise.} \end{cases} \tag{29}$$

where $\emptyset$ means that QPBO fails to label the given vertex.

The utility of QPBO is determined by the number of vertices that the approach fails to label. Experimentally, it has been verified by Rother et al (2007) that if the number of nonsubmodular terms in the energy function is large, the output of QPBO contains many unlabeled vertices (Rother et al (2007) reported that up to 99.9% of variables could be undetermined). However, a promising approach to resolve this problem is the extended roof duality presented by Boros et al (2006). Rother et al (2007) also reviewed the extended

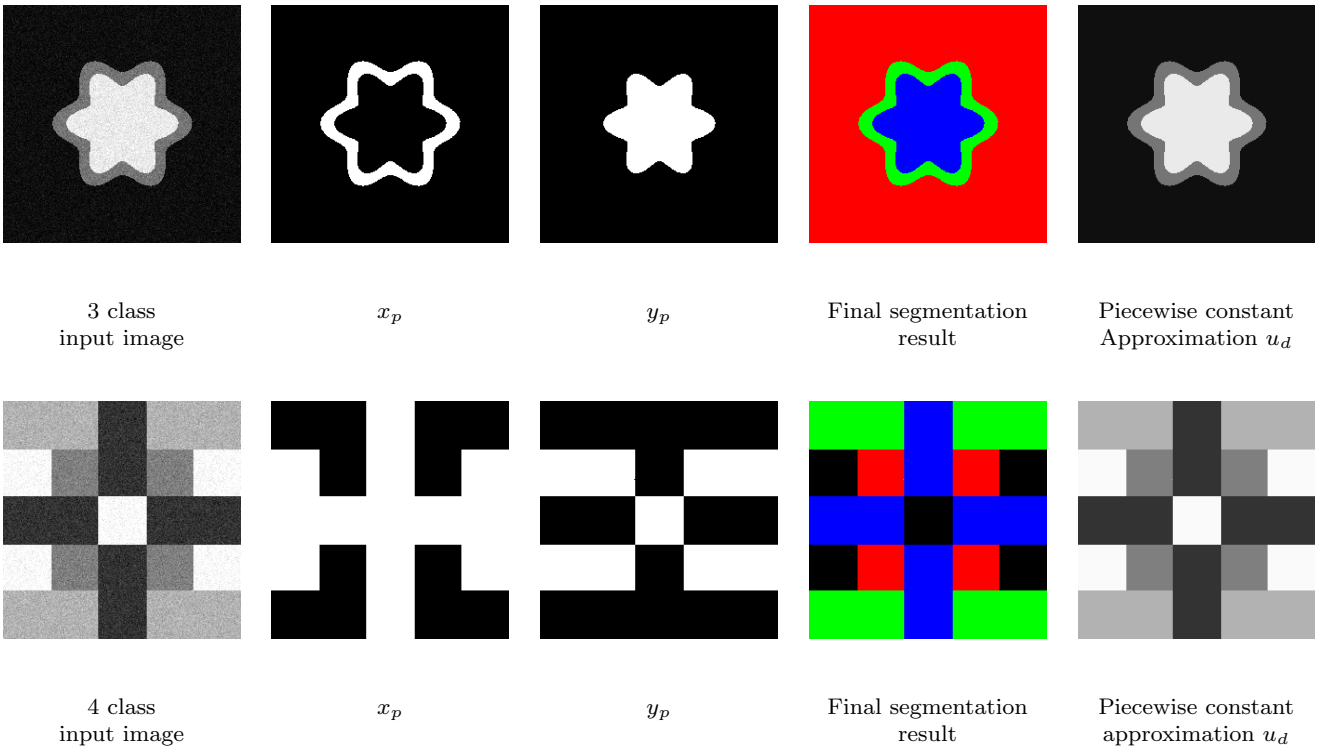

Fig. 3 Three and four class segmentation via binary classifications on a two layer graph. The first column contains the input images. The second column shows the labeling of the vertices in layer 1 of the graph. The third column shows the labeling of the vertices in layer 2 of the graph. The fourth column shows the final segmentation results by combining the labels from the two layers. The last column shows the piecewise constant approximation of the input image.

roof duality approach, first introduced by Boros et al (2006) and presented a more efficient implementation than Boros's. Their work extends QPBO by a probing operation that aims at calculating the global minimum for the vertices that have not been assigned a label by QPBO. The approach is referred to as QPBOP (Quadratic Pseudo Boolean Optimization with Probing). It has been reported by Rother *et al.* that applying QPBOP can reduce the number of unlabeled pixels from 99.9% to 0%.

Next, we will present the graph construction that represents our energy function. Then, we will use QPBO/ QPBOP to partition the constructed graph. This will yield the optimal labeling for X that results in the minimum of our energy functional.

Graph Construction for the energy in (8)

We will construct three graphs $\mathcal{G}_1$, $\mathcal{G}_2$ and $\mathcal{G}_3$ for F_{L1}, F_{L2} and F_{Data}, respectively. Then, we will use the additivity theorem presented by Kolmogorov (2003) to provide the graph $\mathcal{G}$ that represents the discrete energy F_{D}.

Step1: Construct a graph $\mathcal{G}_1 = (\mathcal{V}_1, \mathcal{E}_1)$ with $|\mathcal{V}_1| = M$ such that every pixel p has a corresponding vertex v_p and add the weights as follows: $\forall(p \in \Omega \wedge q \in \mathcal{N}(p))$ add an edge $e_{v_p v_q}$ with weight $w_{v_p v_q}$ to penalize the length of the boundary.

Step 2: Similarly, construct a graph $\mathcal{G}_2 = (\mathcal{V}_2, \mathcal{E}_2)$ with $|\mathcal{V}_2| = M$ such that every pixel p has a corresponding vertex z_p and add the weights as follows: $\forall(p \in \Omega \wedge q \in \mathcal{N})$ add an edge with weight $w_{z_p z_q}$.

Step 3: Construct a 4-partite graph $\mathcal{G}_3 = (\mathcal{V}_1,\mathcal{V}_2,\mathcal{S},\mathcal{T},\mathcal{E}_3)$ with an edge $e_{v_p z_p}$ with weight $w_{v_p z_p} = F_{\mathrm{Data}}(1,1) + F_{\mathrm{Data}}(0,0) - F_{\mathrm{Data}}(0,1) - F_{\mathrm{Data}}(1,0)$. Add an edge $\mathcal{S}v_p$ with weight $w_{\mathcal{S}v_p} = F_{\mathrm{Data}}(1,1)$ - $F_{\mathrm{Data}}(1,0)$ and an edge $z_p\mathcal{T}$ with weight $w_{z_p}\mathcal{T} = F_{\mathrm{Data}}(0,1)$ - $F_{\mathrm{Data}}(1,1)$.

Graphs $\mathcal{G}_1$, $\mathcal{G}_2$ and $\mathcal{G}_3$ are depicted in Figure 2 (a), (b) and (c), receptively. In Figure 2, we use a 4-connected lattice for the ease of illustration, however, all the results in this paper were obtained using an 8-connected lattice. The construction is not limited to lattices. It is general and can be used for arbitrary graphs.

Using the additivity theorem of Kolmogorov (2003), the graph $\mathcal{G} = \{\mathcal{V}, \mathcal{E}\}$ is the graph in which $\mathcal{V} = \mathcal{V}_1 \cup \mathcal{V}_2 \cup \{\mathcal{S}, \mathcal{T}\}$ and $\mathcal{E} = e_{v_p,v_q} \cup e_{z_p,z_q} \cup e_{v_p,z_p}$, with weights collected from $\mathcal{G}_1, \mathcal{G}_2$ and $\mathcal{G}_3$. Note that $\mathcal{E}_1, \mathcal{E}_2$ and $\mathcal{E}_3$ are disjoint, otherwise respective weights have to be added.

After constructing the graph as discussed, we apply QPBO to obtain the labeling. Experimentally, QPBO gives a complete labeling in most of the cases. If QPBO does not provide complete labeling, we apply QPBOP, which found an optimal solution in all of the images that we have segmented. For example, for the sample of the images shown in this paper, QPBO provided complete labeling for 15 out of 16 images and for the one image that QPBO gave partial labeling and failed to label 3% of the vertices, the probing succeeds to label all the vertices that QPBO missed. For segmenting three classes, we simply assign the same data term for two classes and different data terms for the remaining two. Figure 3 illustrates the segmentation of a three class image and a four class image. The figure depicts the binary labeling in each layer of the graph and the final segmentation obtained by combining the binary labeling of the two layers.

2.6 Extension to more than 4 classes

To extend the model to more than four classes, we could simply add extra layers in the graph. For example to compute a segmentation into 8-classes, each pixel p should be associated with a binary vector of three components $Xp = [x_p\ y_p\ z_p]$. The piecewise constant data model for the eight classes is expressed as:

$$\begin{aligned} F_{\text{Data}} = & (u(p) - c_{111})^2 x_p y_p z_p \\ & + (u(p) - c_{110})^2 x_p y_p (1 - z_p) \\ & + (u(p) - c_{101})^2 x_p (1 - y_p) z_p \\ & + (u(p) - c_{110})^2 x_p y_p (1 - z_p) \\ & + (u(p) - c_{011})^2 (1 - x_p) y_p z_p \\ & + (u(p) - c_{101})^2 x_p (1 - y_p) z_p \\ & + (u(p) - c_{100})^2 x_p (1 - y_p)(1 - z_p) \\ & + (u(p) - c_{000})^2 (1 - x_p)(1 - y_p)(1 - z_p) \end{aligned} \tag{30}$$

Unfortunately, the extension to higher than four classes poses a new challenge. The interactions are no longer pairwise in the 8 classes formulation, we have triple interactions and generally the order of the interaction is equal to the number of layers in the graph. The optimization of the energy function with such high interactions becomes more difficult. We examined two different ways to resolve this problem. 1) Decompose the higher order interactions into pairwise interaction using the approach of Ishikawa (2003) and then use QPBO. 2) Use the generalized roof duality for pseudo boolean optimization presented by Kahl and Strandmark (2011). Unfortunately, both of these possibilities result in a high percentage of unlabeled pixels (more than 30% of the pixels were unlabeled). Generalized roof duality generally managed to label more pixels than applying QPBO on the decomposed energy function. However, it was very slow. One iteration for a 100×100 image takes slightly more than an hour and it does not scale linearly (one iteration for 300×300 image takes over a day). Therefore, we maintain our focus in the experiments on the 3 and 4 label construction.

2.7 Algorithm

Having introduced the mathematical formulation of our proposed solution, the implementation details are summarized as follows: The function will be minimized on a graph $\mathcal{G} = \{\mathcal{V}, \mathcal{E}\}$.
The vertex set $\mathcal{V} = \{v_1, v_2, ..., v_M, z_1, z_2, ..., z_M\} \cup \{\mathcal{S}, \mathcal{T}\}$ where M in the number of pixels in the input data set. *i.e.* each pixel p in the input data set has a two corresponding vertices v_p in the first layer of the graph and z_p in the second layer and $\mathcal{S}$ and $\mathcal{T}$ are auxiliary vertices representing the source and target of the graph, respectively. The edge set $\mathcal{E}$ is subdivided into intra-layer edges that correspond to the regularization and inter-layer links that represent the data fidelity. Pseudo code of the algorithm is given in Algorithm 1. The pseudo code is written for the simplest data term F_{DataPC} but it can be easily generalized to F_{DataPS} and F_{DataVV}.

Notice that the the optimization of the Mumford-Shah model is performed in an alternating iterative scheme where we solve for the labels to update the means to formulate a new energy. In the boundary optimization problem that we are solving, when QPBO /QPBOP returns a label, it's the global optimum and in all of our experiments QPBOP provided complete labeling (*i.e.* For each iteration in our scheme, we obtain a complete global solution for the boundary optimization component of minimizing the piecewise constant MS functional).

3 Experimental Results and Discussion

This section presents the experimental results for the proposed approach on synthetic and real images. It also presents the results of brain tissue classification in magnetic resonance images using the proposed multiphase segmentation.

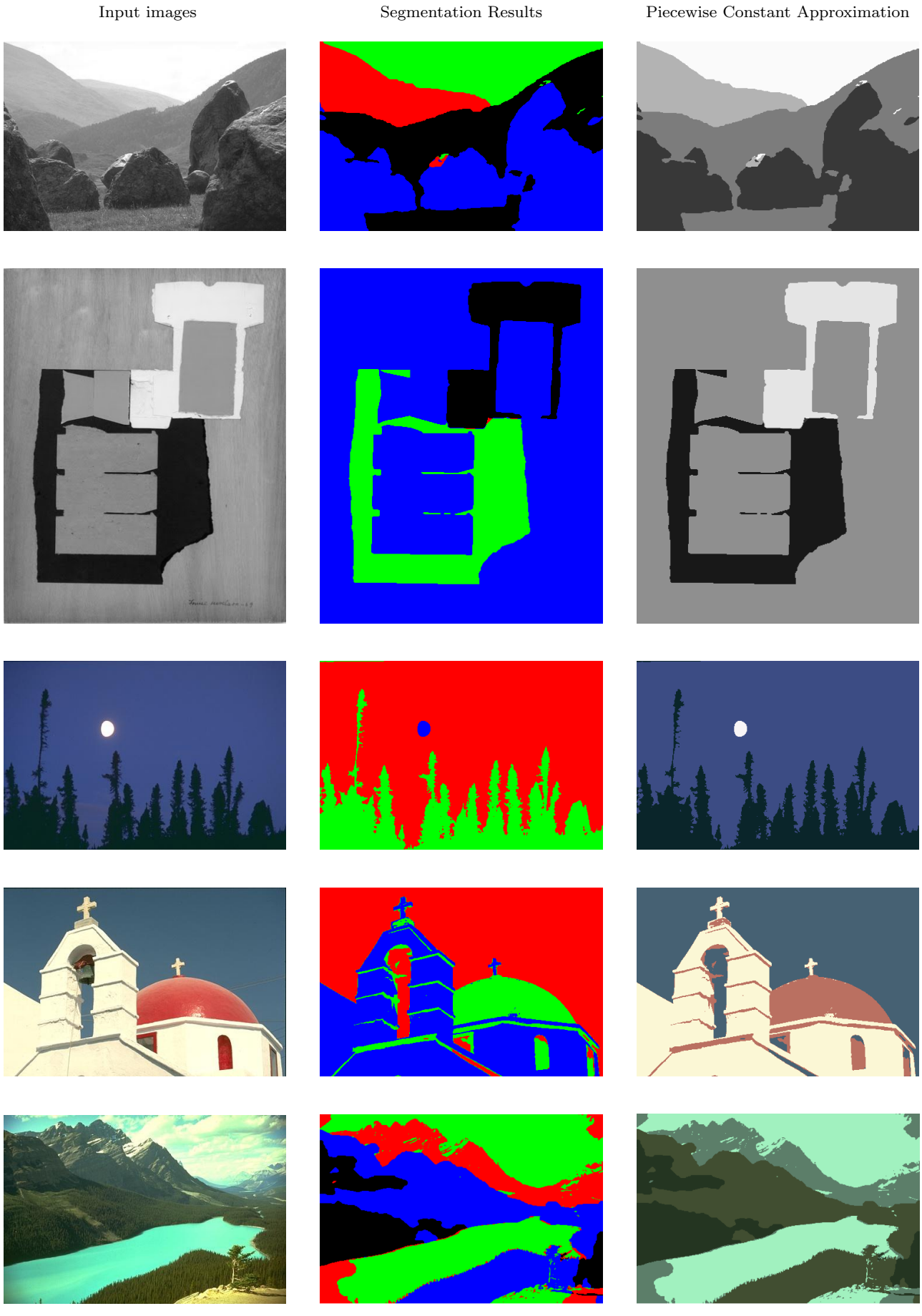

Fig. 4 First column: The input images. Second column: segmentation results. Third column: The piecewise constant Approximation.

QPBO for the multiphase Mumford-Shah image segmentation and denoising

Input: A set of points $p \in \Omega$ with associated feature $u(p)$
Output: Labeling $l(p)$ $\forall p \in \Omega$ and $l \in \{l_1, l_2, l_3, l_4\}$

begin

1. INITIALIZE the variables x_p and y_p $\forall p \in \Omega$.

Note: We usually initialize the variables using two intersecting circles as shown in Figure 1 and equations (4) and (5). The circles are centered at $(\frac{M}{2}, \frac{N}{3})$ and $(\frac{M}{2}, \frac{2N}{3})$ where M and N are the number of rows and columns in the image, respectively. The radii are arbitrary.

Calculate c_{11}, c_{01}, c_{10} and c_{11} using (12) to (15)

while $F^{i+1} - F^i > \epsilon$ **do**

2. ADDING data fidelity edges

- Add an edge $e_{v_p z_p}$ with weight w_{v_p,z_p}= $(u(p) - c_{11})^2$- $(u(p) - c_{01})^2$- $(u(p) - c_{10})^2$ + $(u(p) - c_{00})^2$
- Add an edge $e_{\mathcal{S}v_p}$ with weight $w_{\mathcal{S}v_p}$= $(u(p) - c_{11})^2 - (u(p) - c_{10})^2$.
- Add an edge $e_{z_p\mathcal{T}}$ with weight $w_{z_p\mathcal{T}}$=$(u(p) - c_{01})^2 - (u(p) - c_{11})^2$

3. ADDING boundary regularization

$\forall p, q \in \Omega$

- Add an edge $e_{v_p v_q}$ with weight $w_{v_p v_q}$
- Add an edge $e_{z_p z_q}$ with weight $w_{z_p z_q}$

4. OPTIMIZE: Apply QPBO/QPBOP of Rother et al (2007) to find the min cut $\mathcal{C}$ of the graph $\mathcal{G}$.

FIND LABELS QPBO/QPBOP provides the labels for x_p and y_p. The binary combinations of x_p and x_q gives the labels l_1, l_2, l_3 and l_4.

5. UPDATE means Calculate c_{00}, c_{01}, c_{10} and c_{11} using equations (12), (13), (14) and (15).

end

end

Algorithm 1: Algorithm for the discrete optimization for the discretized multiphase Mumford-Shah model.

3.1 Results Using Piecewise Constant Approximation on Scalar Images

Figure 3 depicts the results of optimizing the 4-class Mumford-Shah functional with the data term F_{DataPC} on two images, the first contains three classes and the second contains four classes. The second and the third columns of the figure shows the labeling of each layer in the graph (*i.e.* the values of x_p and y_p), the fourth column shows the final segmentation results (*i.e.* the labels l_1, l_2, l_3 and l_4) obtained by combining the labels of the two layers. The last column shows the piecewise constant approximation of each image obtained using (16) which may be viewed as a denoised version of the input image. The first two rows of Figure 4 shows our segmentation results for real input images. The rocks image from the Berkley Segmentation Data Set of Martin et al (2001) and a painting for Louise Nevelson (www.theartstory.org). Third, fourth and fifth rows are vector-valued (RGB) images. The first column shows the input images, the second and third columns display the final segmentation results and the piecewise constant approximation, respectively.

3.2 Results Using Piecewise Constant Approximation on Vector Valued Images

Figure 5 shows an example of a vector-valued image where there are three channels that represent the same image. We simulated an image with two objects (ellipse and triangle) and added Guassian noise to each channel, every image (channel) contains partial information about each object, for example, each channel has a missing corner of the triangle. The objects can not be correctly segmented from a single channel but integrating the information from the different channels results in the correct segmentation as depicted in Figure 5 (d). The piecewise constant approximation of the image is a denoised representation of the input in all the channels.

Another example of vector valued image segmentation is the segmentation of RGB images where every color channel represent a component in the vector. The third to fifth rows of Figure 4 depict our segmentation results of real color images from the Berkley Segmentation Data Set. The image in Figure 4 in the third row illustrates an example that results in frustrated cycles in the construction presented by Delong and Boykov (2009) (the sky class contains the moon and the trees. the moon class excludes the trees class) but in our construction (given c_{00}, c_{01}, c_{10}, c_{11}), QBPO provided a complete labeling which guarantees an optimal solution.

3.3 Results using the locally constant approximation

To test our approach for the segmentation of inhomogeneous images, we have simulated images where the

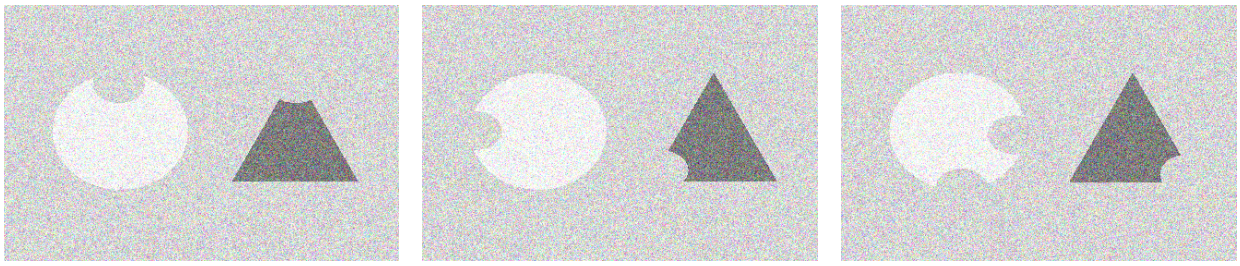

(a) Channel 1 (b) Channel 2 (c) Channel 3

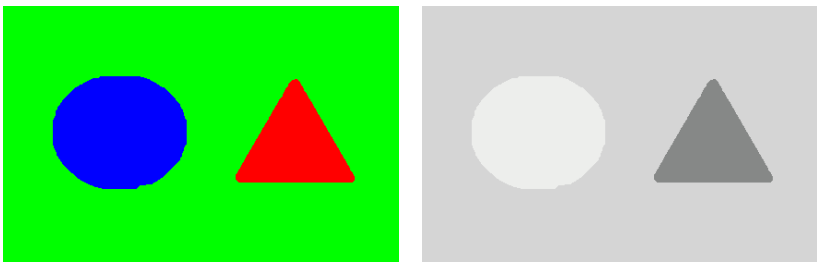

(d) Final Segmentation (e) Piecewise constant approximation of the input image

Fig. 5 Segmentation of an image from three different channels. Each channel contains different information. (a)-(c) The three input channels. (d) The final segmentation using the vector valued data model. (e) The piecewise constant approximation of the input channels that represents a denoised reconstruction of the input vector.

independent objects have high intensity variations. For example, the first image in Figure 6 depicts an ellipse where the boundaries are much brighter than the center and a triangle that is much darker at the top. The segmentation algorithm manages to classify each object correctly. This result is interesting because when we start the algorithm with four classes, the algorithm does not split inhomogeneous classes but rather results in the correct classification with three meaningful classes and an empty class.

The second image is taken from the IBSR data set (Kwan et al (1999)) for a phantom that simulates the noise and inhomogeneity field associated with brain MRI images. The correct classification is obtained and the smooth approximation of the image is treated as a denoised version of the input image.

3.4 Application to MRI Tissue Classification

Tissue classification in brain magnetic resonance images is a potential application that can highly benefit from this approach. The classification algorithm should subdivide the image into four classes; background, gray matter, white matter and cerebrospinal fluid. We have applied our optimization of the multiphase Mumford-Shah to MRI images from the BrainWeb simulated data set in Collins et al (1998). Figure 8 depicts a sample of our results for MRI tissue classification. The first row shows three T1-weighted MRI slices in axial, coronal and sagittal views, respectively. The second row displays the corresponding segmentation. The third row shows three slices in the different views for T2-weighted MRI and their segmentation results are depicted in the fourth row.

To validate our approach, we run our formulation of the discretized Mumford-Shah segmentation algorithm on 100 images out of the simulated Brainweb data set. We repeated the experiments 8 times with different regularization strength as we change ν_1 and ν_2 from 0.001 to 10000. In the 800 trials, we obtained complete labeling which demonstrates the efficiency of QPBOP, even when a high regularization parameter was used.

Figure 7 shows a scatter plot of the number of unlabeled variables using QPBO and the extra time needed by the probing to label these variables.

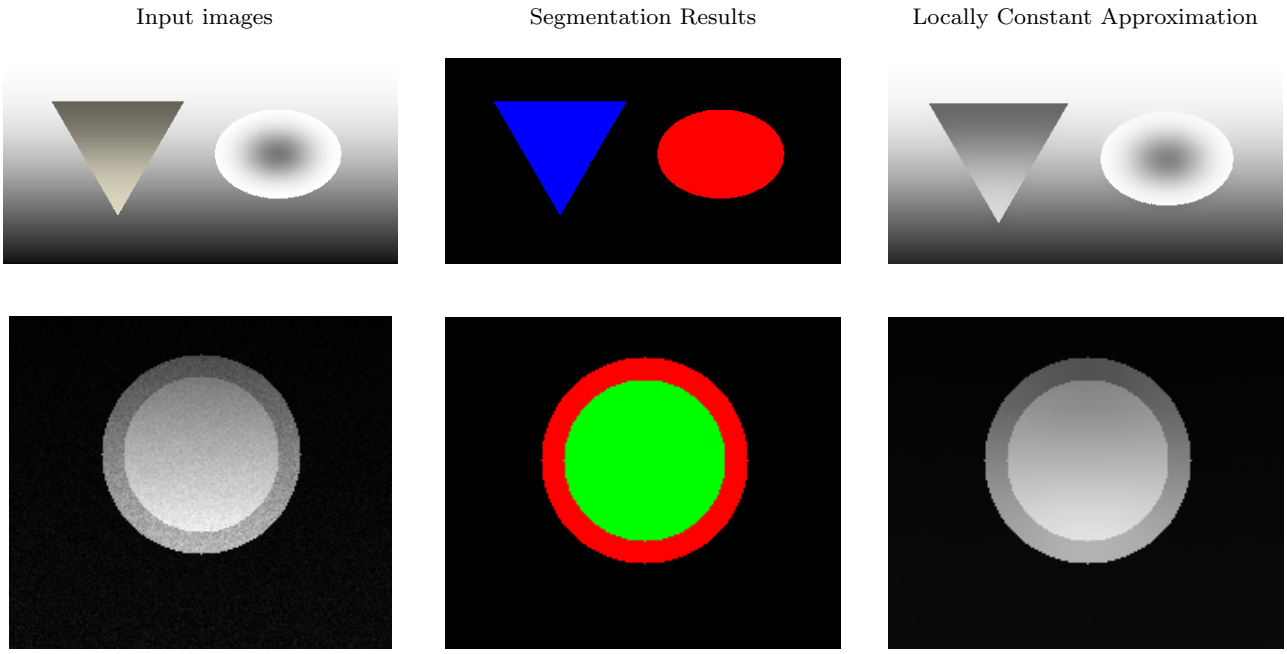

Fig. 6 First column: The input images. Second column: segmentation results. Third column: The locally constant approximation.

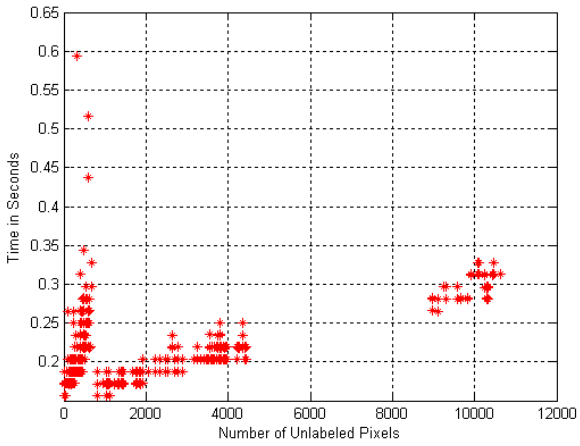

Fig. 7 Number of unlabeled variables using QPBO versus the probing time.

4 Conclusion

Vese and Chan (2002) presented a level set numerical implementation for the multiphase Mumford-Shah model and promoted its applicability to image segmentation. Later research papers investigated more efficient implementations for the model. However, these studies provided solutions that are slow, local and require good initialization to produce a good segmentation. Previous discrete formulations for Mumford-Shah functional apply recursive bisection that uses the 2-phase Mumford - Shah as a core for the segmentation algorithm which affects the robustness of the segmentation whether the optimization is continuous or discrete. This paper provided a discrete formulation for the multiphase Mumford - Shah functional (up to four classes) that does not require recursive bisection and provides a globally optimal solution in practice. Most of the previous work avoids nonsubmodularity and exerts their efforts towards formulating the multiphase segmentation problem in a submodular domain. But, our algorithm deals with the nonsubmodularity using QPBO/QPBOP which are very efficient tools that, in practice, provided a globally optimal solution over all 800 segmentation trials. The data terms presented in the paper can handle inhomogeneous images and can segment vector valued images. We presented our observations on extending the model to more than four classes, but a resolution to the nonsubmodularity of this problem remains open for future work.

References

Badshah N, Chen K (2009) On two multigrid algorithms for modeling variational multiphase image segmentation. IEEE Transaction on Image Processing 18(5):1097–1106

Bae E, Tai XC (2009a) Efficient global minimization for the multiphase Chan-Vese model of image segmentation. In: International Conference on Energy Mini-

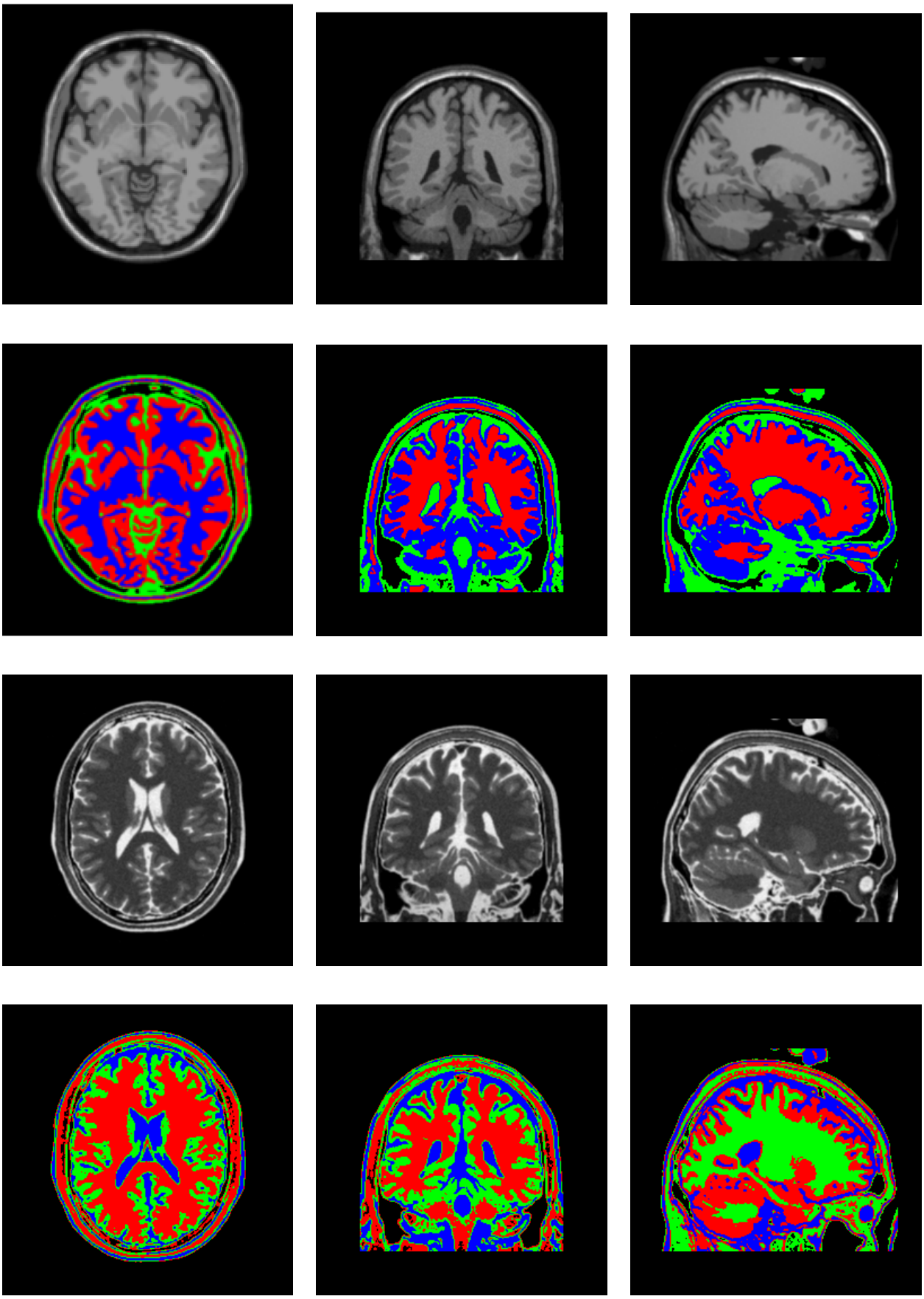

Fig. 8 Sample of the segmentation results of T1 and T2 weighted MRI brain slices in coronal, sagittal and axial views.

mization Methods in Computer Vision and Pattern Recognition, EMMCVPR '09, pp 28–41

Bae E, Tai XC (2009b) Graph cut optimization for the piecewise constant level set method applied to multiphase image segmentation. In: International Conference of Scale Space and Variational Methods in Computer Vision, pp 1–13

Bae E, Yuan J, Tai XC (2011) Global minimization for continuous multiphase partitioning problems using a dual approach. International Journal of Computer Vision 92(1):112–129

Boros E, Hammer PL, Tavares G (2006) Preprocessing of unconstrained quadratic binary optimization. Tech. Rep. RRR 10-2006, RUTCOR

Boykov Y, Veksler O, Zabih R (1999) Fast approximate energy minimization via graph cuts. In: International Conference for Computer Vision, ICCV99, vol 1, pp 377–384

Bresson X, Esedognlu S, Vandergheynst P, Thiran JP, Osher S (2007) Fast global minimization of the active contour/snake model. Journal of Mathematical Imaging and Vision 2:151–167

Brown E, Chan T, Bresson X (2010) A convex approach for multiphase piecewise constant Mumford-Shah image segmentation. Tech. Rep. CAM 09-66, UCLA

Bruckstein A, Netravali A, Richardson (1997) Epi-convergence of discrete elastica. Applicable Analysis 79(1-2):137–171

Chan TF, Vese LA (2001) Active contours without edges. IEEE Transation on Image Processing 10(2):266–277

Chung G, Vese LA (2005) Energy minimization based segmentation and denoising using a multilayer level set approach. In: International Conference on Energy Minimization Methods in Computer Vision and Pattern Recognition, pp 439–455

Collins DL, Zijdenbos AP, Kollokian V, Sled JG, Kabani NJ, Holmes CJ, Evans AC (1998) Design and construction of a realistic digital brain phantom. IEEE Transactions on Medical Imaging 17(3):463–468

Darbon J, Sigelle M (2005) A fast and exact algorithm for total variation minimization. In: IbPRIA (1), pp 351–359

Delong A, Boykov Y (2009) Global optimal segmentation of multi-region objects. In: International Conference on Computer Vision, vol 1, pp 26–33

El-Zehiry N, Elmaghraby A (2008) A graph cut based active contour without edges with relaxed homogeneity constraint. In: International Conference on Pattern Recognition, pp 1–4

El-Zehiry N, Xu S, Sahoo P, Elmaghraby A (2007) Graph cut optimization for the mumford-shah model. In: International Conference on Visualization, Imaging and Image Processing, pp 182–187

El-Zehiry N, Sahoo P, Elmaghraby A (2011) Combinatorial optimization of the piecewise constant Mumford-Shah functional with application to scalar/vector valued and volumetric image segmentation. Image and Vision Computing 29:365–381

El-Zehiry NY (2009) A graph cut framework for two dimensional/three dimensional implicit front propagation with application to the image segmentation problem. PhD thesis, Louisville, KY, USA

El-Zehiry NY, Elmaghraby A (2007) Brain MRI tissue classification using graph cut optimization of the Mumford-Shah functional. In: Inernational Vision Conference of New Zealand, New Zealnd, pp 321–326

Grady L, Alvino C (2009) The piecewise smooth Mumford-Shah functional on an arbitrary graph. IEEE Transaction on Image Processing 18(11):2547–2561

Grady L, Polimeni JR (2010) Discrete Calculus: Applied Analysis on Graphs for Computational Science. Springer

Hammer PL, Hansen P, Simeone B (1984) Roof duality, complementation and persistency in quadratic 01 optimization. Mathematical Programming 28(2):121–155

Ishikawa H (2003) Exact optimization for Markov random fields with convex priors. IEEE Transaction on Pattern Analysis and Machine Intelligence 25:1333–1336

Jeon M, Alexander M, Pedrycz W, Pizzi N (2005) Unsupervised hierarchical image segmentation with level set and additive operator splitting. Pattern Recognition Letters 26:1461–1469

Kahl F, Strandmark P (2011) Generalized roof duality for pseudo-boolean optimization. In: International Conference on Computer Vision, pp 255–262

Kohli P, Kumar MP, Torr PHS (2009) P & beyond: Move making algorithms for solving higher order functions. IEEE Transaction on Pattern Analysis and Machine Intelligence 31(9):1645–1656

Kolmogorov V (2003) Graph based algorithms for scene reconstruction from two or more views. PhD thesis, Cornell University

Kolmogorov V, Boykov Y (2005) What metrics can be approximated by geo-cuts, or global optimization of length/area and flux. In: International Conference on Computer Vision, ICCV05, vol 1, pp 564–571

Kolmogorov V, Rother C (2007) Minimizing nonsubmodular functions with graph cuts-a review. IEEE Transaction on Pattern Analysis and Machine Intelligence 29(7):1274–1279

Kolmogorov V, Zabih R (2004) What energy functions can be minimized via graph cuts? IEEE Transaction on Pattern Analysis and Machine Intelligence 26(2):147–159

Komodakis N, Tziritas G (2007) Approximate labeling via graph cuts based on linear programming. IEEE Transaction on Pattern Analysis and Machine Intelligence 29(8):1436–1453

Kwan RS, Evans A, Pike G (1999) MRI simulation-based evaluation of image-processing and classification methods. IEEE Transactions on Medical Imaging 18(11):1085–1097

Lellmann J, Becker F, Schnörr C (2009) Convex optimization for multi-class image labeling with a novel family of total variation based regularizers. In: International Conference on Computer Vision, pp 646–653

Martin D, Fowlkes C, Tal D, Malik J (2001) A database of human segmented natural images and its application to evaluating segmentation algorithms and measuring ecological statistics. In: International Conference on Computer Vision, vol 2, pp 416–423

Mumford D, Shah J (1988) Optimal approximations by piecewise smooth functions and variational problems. Communications of Pure and Applied Mathematics XLII(5):577–685

Ni K, Hong BW, Soatto S, Chan T (2009) Unsupervised multiphase segmentation: A recursive approach. Computer Vision and Image Understanding 113(4):502–510

Osher S, Sethian JA (1988) Fronts propagating with curvature-dependent speed: algorithms based on hamilton-jacobi formulations. J Comput Phys 79(1):12–49

Pock T, Schoenemann T, Graber G, Bischof H, Cremers D (2008) A convex formulation of continuous multi-label problems. In: European Conference on Computer Vision, pp 792–805

Pock T, Cremers D, Bischof H, Chambolle A (2009) An algorithm for minimizing the Mumford-Shah functional. In: International Conference on Computer Vision, pp 1133–1140

Ramalingam S, Kohli P, Alahari K, Torr PHS (2008) Exact inference in multi-label CRFs with higher order cliques. In: IEEE Conference on Computer Vision and Pattern Recognition, pp 1–8

Rother C, Kolmogorov V, Lempitsky V, Szummer M (2007) Optimizing binary MRFs via extended roof duality. In: IEEE conference on Computer Vision and Pattern Recognition, vol 5302, pp 248–261

Simon H, Teng SH (2001) How good is recursive bisection? SIAM Journal on Scientific Computing 18(5):1436–1445

Vazquez-Reina A, Miller E, Pfister H (2009) Multiphase geometric couplings for the segmentation of neural processes. IEEE Conference Computer Vision and Pattern Recognition pp 2020–2027

Vese LA, Chan TF (2002) A multiphase level set framework for image segmentation using the Mumford and Shah model. International Journal of Computer Vision 50(3):271–293

Wainwright M, Jaakkola T, Willsky A (2002) MAP estimation via agreement on (hyper)trees: Message-passing and linear programming approaches. IEEE Transactions on Information Theory 51:3697–3717

Yuan J, Bae E, Boykov Y, Tai XC (2011) A continuous max-flow approach to minimal partitions with label cost prior. In: Scale Space and Variational Methods in Computer Vision, pp 279–290